1   RUNNING TITLE: Hyporheic zone hotspot mechanisms

2

3   Multi 'omics comparison reveals metabolome biochemistry, not microbiome composition or

4   gene expression, corresponds to elevated biogeochemical function in the hyporheic zone

5

6   Emily B. Graham[1], Alex R. Crump[2], David W. Kennedy[1], Evan Arntzen[1], Sarah Fansler[1],

7   Samuel O. Purvine[3], Carrie D. Nicora[3], William Nelson[1], Malak M. Tfaily[3], and James C.

8   Stegen[1]

9

10   [1]Pacific Northwest National Laboratory, Richland, WA USA

11   [2]University of Idaho, Moscow, ID USA

12   [3]Environmental Molecular Science Laboratory, Richland, WA USA

13

14   **Correspondence:** Emily B. Graham, Pacific Northwest National Laboratory, PO Box 999,

15   Richland, WA 99352, 509-372-6049, emily.graham@pnnl.gov

16

19

20

21 **Abstract.**

22   Biogeochemical hotspots are pervasive at terrestrial-aquatic interfaces, particularly within

23 groundwater-surface water mixing zones (hyporheic zones), and they are critical to

24 understanding spatiotemporal variation in biogeochemical cycling. Here, we use multi 'omic

25 comparisons of hotspots to low-activity sediments to gain mechanistic insight into hyporheic

26 zone organic matter processing. We hypothesized that microbiome structure and function, as

27 described by metagenomics and metaproteomics, would distinguish hotspots from low-activity

28 sediments through a shift towards carbohydrate-utilizing metabolic pathways and elucidate

29 discrete mechanisms governing organic matter processing in each location. We also expected

30 these differences to be reflected in the metabolome, whereby hotspot carbon (C) pools and

31 metabolite transformations therein would be enriched in sugar-associated compounds. In contrast

32 to expectations, we found pronounced phenotypic plasticity in the hyporheic zone microbiome

33 that was denoted by similar microbiome structure, functional potential, and expression across

34 sediments with dissimilar metabolic rates. Instead, diverse nitrogenous metabolites and

35 biochemical transformations characterized hotspots. Metabolomes also corresponded more

36 strongly to aerobic metabolism than bulk C content only (explaining 67% vs. 42% of variation),

37 and bulk C did not improve statistical models based on metabolome composition alone. These

38 results point to organic nitrogen as a significant regulatory factor influencing hyporheic zone

39 organic matter processing. Based on our findings, we propose incorporating knowledge of

40 metabolic pathways associated with different chemical fractions of C pools into ecosystem

41 models will enhance prediction accuracy.

42 **1. Introduction.**

43   Soils and nearshore sediments contain a vast reservoir of stored carbon. Uncertainty in

44 the fate of these stores is central to constraining future atmospheric CO_2 concentrations (Burd et

45 al., 2016; Luo et al., 2016; Todd-Brown et al., 2013). Advances in molecular technology has

46 given researchers new ability to characterize mechanisms governing carbon (C) bioavailability,

47 and ultimately the conversion of belowground C pools to CO_2. These advances are central to

48 ongoing efforts to improve process-based ecosystem models by incorporating microbial and

49 biochemical complexity in biogeochemical processes (Buchkowski et al., 2017; Luo et al., 2016;

50 Wieder et al., 2013; Wieder et al., 2017). Still, there is little consensus on the roles of diverse

51 environmental and microbial factors in enhancing belowground CO_2 flux predictions (Graham et

52 al., 2016b; Graham et al., 2014; Luo et al., 2016; Rocca et al., 2015; Wieder et al., 2017), and

53 understanding the mechanisms regulating biogeochemistry in natural environments is paramount

54 to conceptualizing the structure and parameterization of models (Luo et al., 2016; Todd-Brown

55 et al., 2013; Wieder et al., 2013).

56   Recent research has vastly improved both molecular methodologies (Aebersold and

57 Mann, 2003; Gabor et al., 2014; Tfaily et al., 2017; Tringe and Rubin, 2005; Viant, 2008; Wang

58 et al., 2009) and biogeochemical mechanisms represented in ecosystem models (Allison et al.,

59 2010; Wieder et al., 2015a; Wieder et al., 2013; Xu et al., 2014). For instance, parallel advances

60 in environmental chemistry and microbiology now allow for detailed characterization of

61 belowground C pools (e.g., fluorescent methods (Gabor et al., 2014), high-resolution mass

62 spectroscopy (Tfaily et al., 2017), and nuclear magnetic resonance (NMR) (Markley et al.,

63 2017)) as well as the structure and function of environmental microbiomes (Aebersold and

64 Mann, 2003; Tringe and Rubin, 2005; Wang et al., 2009). Newly improved process models

65   account for chemical attributes of C (Liski et al., 2005; Wang et al., 2017), microbial biomass

66   and physiology (Wieder et al., 2014; Wieder et al., 2015a), and nutrient limitations (Wieder et

67   al., 2015b) in their representations of biogeochemistry, among other factors (Verheijen et al.,

68   2015; Wang et al., 2017). Despite these advances, cross-system experimental evidence has

69   revealed many inconsistencies in the importance of different biogeochemical and microbial

70   properties explaining respiration rates (Graham et al., 2016b; Graham et al., 2017b; Hartman et

71   al., 2017), suggesting a need for greater spatially-explicit understanding of mechanisms involved

72   in organic matter processing (Graham et al., 2017b; Krause et al., 2017).

73   Terrestrial-aquatic interfaces are recognized active regions of C metabolism, and areas of

74   subsurface groundwater-surface water mixing (hyporheic zones) in particular are critical in

75   determining the fate of organic matter globally (Battin et al., 2009; Boulton et al., 1998; Cole et

76   al., 2007; Marín-Spiotta et al., 2014; Regnier et al., 2013). Hyporheic zones contribute

77   disproportionately to stream and river metabolism (Gomez-Velez et al., 2015; Huizenga et al.,

78   2017; Stegen et al., 2016; Stern et al., 2017), with up to 96% of ecosystem metabolism occurring

79   in this zone in some headwater systems (Naegeli and Uehlinger, 1997). Hotspots and hot

80   moments of enhanced biogeochemical activity at confined locations or time points are common

81   within the hyporheic zone (Boulton et al., 1998; Krause et al., 2017; McClain et al., 2003). These

82   hotspots often correspond to vegetation patterns (Harms and Grimm, 2008; McClain et al., 2003;

83   Schade et al., 2001) and understanding their drivers is critical to accurately representing organic

84   matter decomposition within ecosystem models.

85   Our objective is to determine molecular mechanisms associated with hotspots of aerobic

86   metabolism in the hyporheic zone. Previous work in this system has shown differences in (1)

87   aerobic metabolism across variable mixing of water bodies with distinct C chemistries (Stegen et

88   al., 2016; Stegen et al., 2018) and (2) metabolic processes associated with C oxidation in the

89   presence or absence of vegetation (Graham et al., 2017b). Recent work has also shown that

90   elevated rates of metabolism globally correspond to carbohydrate metabolism in soil

91   metagenomes (Hartman et al., 2017). Based on this research, we hypothesize that microbiome

92   structure and function support elevated carbohydrate metabolism in hyporheic zone hotspots,

93   resulting in higher rates of aerobic metabolism. We expect this dynamic to be reflected in

94   sediment metagenomes, metaproteomes, and metabolomes, whereby hotspot microbiome

95   composition, protein expression, and metabolites are enriched in sugar-associated pathways and

96   compounds, relative to low-activity sediments.

97

98   **2. Materials and Methods.**

99   *2.1. Site Description*

100   This study was conducted along the Columbia River shoreline within the Hanford 300

101   Area (approximately 46° 22' 15.80"N, 119° 16' 31.52"W) in eastern Washington State (Graham

102   et al., 2016a; Graham et al., 2017a; Graham et al., 2017b; Slater et al., 2010; Zachara et al.,

103   2013). The Columbia River experiences shoreline geographic variation in vegetation patterns,

104   substrate geochemistry, microbiome composition, and rates of biogeochemical activity (Arntzen

105   et al., 2006; Graham et al., 2017b; Lin et al., 2012; Peterson and Connelly, 2004; Slater et al.,

106   2010; Stegen et al., 2016; Stegen et al., 2012; Zachara et al., 2013); constituting an ideal system

107   for examining mechanisms associated with biogeochemical hotspots.

108   Liquid N_2-frozen sediment profiles (0-60 cm) were collected along two shoreline

109   transects perpendicular to the Columbia River in March 2015, separated by a distance of ~170m.

110   We collected profiles at three locations in each transect with 5m spacing within a spatial domain

111   of ~175 x 10m. In each transect, the lower bank profile was located at ~0.5m (vertical distance)

112   below the water line and the upper bank profile was located ~0.5m (vertical distance) above the

113   water line (approximately 10m horizontal distance), with the third profile situated at the

114   midpoint. Each profile was sectioned into 10-cm intervals from 0-60cm. To capture a range of

115   biogeochemical activities, one transect had dense vegetation, consisting of a closed canopy of

116   woody perennials *Morus rubra* (Red Mulberry) and *Ulmus rubra* (Slippery Elm), and one

117   transect was characterized by a cobbled armor layer with virtually no vegetation.

118

119   *2.2. Sample Collection*

120   Liquid N_2-frozen sediment profiles were collected as outlined in Moser et al. (2003)

121   using a method modified from Lotspeich and Reed (1980) and Rood and Church (1994). A

122   pointed stainless steel tube (152 cm length, 3.3 cm outside diameter, 2.4 cm inside diameter) was

123   driven into the river bed to a depth of ~60cm. Liquid N_2 was poured down the tube for ~15

124   minutes, until a sufficient quantity of material had frozen to the outside of the tube. The tube and

125   attached material were removed from the riverbed with a chain hoist suspended beneath a tripod.

126   Profiles were placed over an aluminum foil lined cooler containing dry ice. Frozen material was

127   removed with a mallet. The material was then wrapped in the foil and transported on dry ice to

128   storage at -80°C. In the lab, profiles were sectioned into 10cm depth intervals from 0-60 cm (n =

129   6 per profile, except for the unvegetated upper bank profile which was sectioned only from 30-

130   60cm; total n = 33)

131

132   *2.3. Physicochemistry*

133   Details concerning physicochemical assays are provided in the Supporting Information.

134   Briefly, we determined the particle distribution of sediments by separating size fractions via

135   sieving; total nitrogen, sulfur, and carbon content were determined using an Elementar vario EL

136   cube (Elementar Co.Germany); NH_4^+ was extracted with KCl and measured with Hach Kit

137   2604545 (Hach, Loveland, Co); iron content was measured with a ferrozine assay; and all other

138   ion concentrations were measured by inductively coupled plasma mass spectrometry (ICP-MS)

139   on HCl extractions. Aerobic metabolism was determined with a resazurin reduction assay,

140   modified from *Haggerty et al.*(2009). Data are provided in Fig. S1-S3.

141

142   *2.4. FT-ICR-MS solvent extraction and data acquisition*

143   We leverage state of science chemical extraction protocols combined with Electrospray

144   ionization (ESI) and Fourier transform ion cyclotron resonance (FT-ICR) mass spectrometry

145   (MS) to infer differences in metabolites among our samples. ESI FT-ICR-MS introduces intact

146   organic molecules into the MS without fragmentation and allows for the detection of a wide

147   range of chemical compounds (Tfaily et al., 2015; Tfaily et al., 2017). The use of 12 Tesla (T)

148   FT-ICR-MS offers high mass resolving power (>1M) and mass measurement accuracy (<1 ppm),

149   and while nascent in its application within complex environmental systems, it has emerged as a

150   robust method for determining the chemistry of natural organic compounds (Kim et al., 2003;

151   Koch et al., 2005; Tfaily et al., 2011; Tremblay et al., 2007). Additionally, Tfaily et al. (2015;

152   2017) have optimized metabolite characterization from soils and sediments by sequential

153   extraction with polar and non-polar solvents tailored to the sample set of interest. Tfaily's

154   extraction procedures have been coupled to ESI FT-ICR-MS to distinguish metabolites among

155   ecosystems and soil types (Tfaily et al., 2015; Tfaily et al., 2017) as well as to provide

156   information on the utilization of distinct metabolites among samples within a single environment

157   (Bailey et al., 2017; Graham et al., 2017b; Stegen et al., 2018).

158   Here, we used three solvents with different polarities —water (H_2O), methanol (CH_3OH,

159   'MeOH') and chloroform ($CHCl_3$)—to sequentially extract a large diversity of organic

160   compounds from samples, according to Tfaily et al. (2015; 2017). Water extractions were

161   performed first, followed by MeOH and then $CHCl_3$. Previous work has shown that each solvent

162   is selective towards specific types of compounds (Tfaily et al., 2015) and that combining peaks

163   from all extractions provides a more comprehensive description of metabolite composition than

164   any single extraction procedure independently (Tfaily et al., 2017). Water is a polar solvent with

165   a selection bias for carbohydrates with high O/C ratios, amino-sugars, and other labile polar

166   compounds (Tfaily et al., 2015). Conversely, $CHCl_3$ is selective for non-polar lipids associated

167   with mineral interactions and cellular membranes (Tfaily et al., 2015). Methanol has a polarity in

168   between that of water and $CHCl_3$ and extracts a mixture of compounds that water and $CHCl_3$

169   extract (Tfaily et al., 2015). Ultra-high resolution mass spectrometry of the three different

170   extracts from each sample was carried out using a 12 Tesla Bruker SolariX FT-ICR-MS located

171   at the Environmental Molecular Sciences Laboratory (EMSL) in Richland, WA, USA. An

172   expanded description of extraction procedures; instrument calibration and maintenance; and

173   sample injection is presented in the Supplemental Material.

174

175   *2.5. FT-ICR-MS data processing*

176   One hundred forty-four individual scans were averaged for each sample and internally

177   calibrated using an organic matter homologous series separated by 14 Da (–CH_2 groups). The

178   mass measurement accuracy was less than 1 ppm for singly charged ions across a broad *m/z*

179   range (100-1200 m/z). The mass resolution was ~ 350K at 339 m/z. Data Analysis software

180   (BrukerDaltonik version 4.2) was used to convert raw spectra to a list of m/z values applying

181   FTMS peak picker module with a signal-to-noise ratio (S/N) threshold set to 7 and absolute

182   intensity threshold to the default value of 100.

183   For each sample, we combined peaks detected in all three extractions to yield metabolite

184   composition. Peak data were treated as presents/absence data, where a peak was considered to be

185   present in a sample if it was present in at least one of H_2O-, MeOH-, or $CHCl_3$-extracted

186   samples. Presence/absence data were used because peak intensity differences are reflective of

187   ionization efficiency as well as relative abundance (Kujawinski and Behn, 2006; Minor et al.,

188   2012; Tfaily et al., 2015; Tfaily et al., 2017).

189   Putative chemical formulae were then assigned using in-house software following the

190   Compound Identification Algorithm (CIA), proposed by Kujawinski and Behn (2006), modified

191   by Minor et al. (2012), and previously described in Tfaily et al. (2017). Chemical formulae were

192   assigned based on the following criteria: S/N >7, and mass measurement error <1 ppm, taking

193   into consideration the presence of C, H, O, N, S and P and excluding other elements. To ensure

194   consistent formula assignment, we aligned all sample peak lists for the entire dataset to each

195   other in order to facilitate consistent peak assignments and eliminate possible mass shifts that

196   would impact formula assignment. We implemented the following rules to further ensure

197   consistent formula assignment: (1) we consistently picked the formula with the lowest error and

198   with the lowest number of heteroatoms and (2) the assignment of one phosphorus atom requires

199   the presence of at least four oxygen atoms.

200   The chemical character of thousands of peaks in each sample's ESI FT-ICR-MS

201   spectrum was evaluated on van Krevelen diagrams. Compounds were plotted on the van

202   Krevelen diagram on the basis of their molar H:C ratios (y-axis) and molar O:C ratios (x-axis)

203   (Kim et al., 2003). Van Krevelen diagrams provide a means to visualize and compare the average

204   properties of organic compounds and assign compounds to the major biochemical classes (e.g.,

205   lipid-, protein-, lignin-, carbohydrate-, and condensed aromatic-like).

206

207   *2.6. Identification of putative biochemical transformations using FT-ICR-MS*

208   To identify potential biochemical transformations, we followed the procedure detailed by

209   Breitling *et al.* (2006) and employed by Bailey *et al.* (2017), Graham *et al.* (2017b), and Stegen

210   *et al.* (2018). The mass difference between m/z peaks extracted from each spectrum with S/N>7

211   were compared to commonly observed mass differences associated with biochemical

212   transformations. All possible pairwise mass differences were calculated within each extraction

213   type for each sample, and differences (within 1ppm) were matched to a list of 92 common

214   biochemical transformations (e.g., gain or loss of amino groups or sugars, Table S1). For

215   example, a mass difference of 99.07 corresponds to a gain or loss of the amino acid valine, while

216   a difference of 179.06 corresponds to the gain or loss of a glucose molecule. Pairs of peaks with

217   a mass difference within 1 ppm of our transformation list were considered to be related by the

218   corresponding compound. This approach is feasible with FT-ICR-MS data because the set of

219   peaks in each sample are related by measureable and clearly defined mass differences

220   corresponding to gains and losses of compounds.

221

222   *2.7. Metagenome sequencing and annotation*

223   To release biomass from sediment particles, thawed samples were suspended in 20mL of

224   chilled PBS/0.1% Na-pyrophosphate solution and vortexed for 1 min. The suspended fraction

225   was decanted to a fresh tube and centrifuged for 15' at 7000 x g at 10°C. DNA was extracted

226   from the resulting pellets using the MoBio PowerSoil kit in plate format (MoBio Laboratories,

227   Inc., Carlsbad, CA) following manufacturer's instructions, with the addition of a 2-hour

228   proteinase-K incubation at 55°C prior to bead-beating to facilitate cell lysis.

229   Purified genomic DNA was submitted to the Joint Genome Institute under JGI/EMSL

230   proposal 1781 for paired-end sequencing on an Illumina HiSeq 2500 sequencer (Table S2).

231   Reads were processed by BBDuk to remove adapters (ktrim=r, minlen=40, minlenfraction=0.6,

232   mink=11, tbo, tpe, k=23, hdist=1, hdist2=1, ftm=5) and trim for quality <12 (maq=8, maxns=1,

233   minlen=40, minlenfraction=0.6, k=27, hdist=1, trimq=12, qtrim=rl) and screened for

234   contaminants against a masked version of human HG19 using BBMap (fast local minratio=0.84

235   maxindel=6 tipsearch=4 bw=18 bwr=0.18 usemodulo printunmappedcount idtag minhits=1).

236   (BBDuk and BBMap are available at https://sourceforge.net/projects/bbmap) Remaining reads

237   were assembled with megahit (Li et al., 2016) using default parameters and k-list=23,43,63,

238   83,103,123. Gene calling and functional and taxonomic annotation was performed by MGAP

239   v4.11.4 (Huntemann et al., 2015). Data sets are available through the JGI Genome Portal

240   (http://genome.jgi.doe.gov). Project identifiers are listed in Table S2.

241

242   *2.8. Metaproteomics.*

243

244   Sediment samples were prepared for proteome analysis as per Nicora et al. (in press) and

245   detailed below. Additional details are provided in the Supplemental Material.

246   Proteins were extracted from 30 g of lyophilized sediment using MPLex direct SDS

247   buffer extraction. Sediment was weighed into 50 mL screw-cap self-standing tubes (Next

248   Advance, Averill Park, NY) along with 0.9-2.0 mm stainless steel beads, 0.1 mm zirconia beads

249   and 0.1 mm garnet beads and 8 mL of 60% MeOH in nanopure water. The samples were all bead

250   beat in a 50mL Bullet Blender (Next Advance, Averill Park, NY) at speed 12 for 15 minutes at

251   4°C and transferred into chemical compatible polypropylene 50 mL tubes (Olympus Plastics,

252   Waltham, MA). The dirty tube was rinsed with 2 mL of 60% MeOH and combined with the

253   sample along with 12 mL of ice-cold chloroform and probe sonicated at 60% amplitude for 30

254   seconds on ice, allowed to cool on ice and sonicated again. Samples were incubated for 5 min at-

255   80°C, vortexed for 1 min and centrifuged at 4,500x g for 10 min at 4°C. The upper aqueous

256   phase was collected into a large glass vial, being careful not to touch the protein interphase. The

257   interphase was collected using a large flat spatula into a separate tube and 5mL of ice cold 100%

258   methanol was added to the protein, vortexed and centrifuged at 4,500x g for 5 mins at 4°C to

259   pellet the protein. The supernatant was decanted off and the protein allowed to dry upside down

260   on a Kim-wipe. Meanwhile, the bottom organic phase was collected into a separate large glass

261   vial and 5mL of nanopure water was added to the large soil particulates along with 25mL of cold

262   (-20 °C) chloroform:methanol (2:1, v:v) solution and probe sonicated for 30 seconds as

263   described previously. The sample was allowed to cool at -20°C and centrifuged at 4,500x g for

264   10 min at 4°C. The upper aqueous phase metabolites and bottom organic phase lipids were

265   collected together with the supernatant metabolites and lipids then dried down completely in a

266   vacuum concentrator (Labconco, Kansas City, MO) and stored at -20 °C for analysis. The dirty

267   protein interphase had 20 mL of an SDS-Tris buffer (4% SDS, 100mM DTT in 100 mM Tris-

268   HCl, pH 8.0) added and probe sonicated at 20% amplitude to bring into solution and incubated at

269   95°C for 5 minutes to solubilize the protein and allowed to cool for 20 mins at 4°C. The samples

270   were centrifuged at 4,500x g for 10 mins and the supernatants were decanted into chemical

271   compatible polypropylene 50 mL tubes. The proteins were precipitated by adding up to 20%

272   trichloroacetic acid (TCA), vortexed and placed in a -20°C freezer for 1.5 hrs. The samples were

273   thawed and centrifuged at 4,500x g at 4°C for 10 mins to collect the precipitated protein. The

274   supernatant was gently decanted into waste and 2 mL of ice cold acetone was added to the pellet

275   and re-suspend by vortexing. The sample was placed at -80°C for ~5 mins to ensure the samples

276   were cold and centrifuged for 10 mins at 4,500x g at 4°C. The acetone was removed by gently

277   pouring into waste. The pellets were allowed to dry inverted on a Kim Wipe for ~15 mins. The

278   protein interphases from the supernatants and the protein interphases from the particulates were

279   combined using 100-200ul of SDS-Tris buffer and FASP digested (described in the

280   Supplemental Material).

281   Extractions were analyzed on a Q-Exactive Plus mass spectrometer (Thermo Electron,

282   Waltham, MA) coupled to a Waters NanoAcquity high performance liquid chromatography

283   systems (Waters Corporation, Milford, MA) through 75 um x 70 cm columns packed with

284   Phenomenex Jupiter C-18 derivatized 3 um silica beads (Phenomenex, Torrance, CA). Samples

285   were loaded onto columns with 0.05% formic acid in water and eluted with 0.05% formic acid in

286   Acetonitrile over 100 minutes. Ten data-dependent MS/MS scans (17.5K resolution, centroided)

287   were recorded for each survey MS scan (35K resolution) using normalized collision energy of

288   30, isolation width of 2.00, and rolling exclusion window of +/- 1 Th lasting 30 seconds before

289   previously fragmented signals are eligible for re-analysis.

290   For protein identification, a single reference protein file was developed from the

291   combination of 33 metagenome files ('assembled.faa' and 'product_names' files) available from

292   the Joint Genome Institute (JGI Project IDs and related download links in Supplemental

293   Material). Exact sequence duplicates were removed, and 16 commonly observed contaminants

14

294   (e.g. tryptic fragments, human keratins, and serum albumin precursors) were included. Final file

295   contained 10,063,272 protein entries from 1,299,102,456 amino acids, 2.04GB in size.

296   The MS/MS spectra from all LC-MS/MS datasets were converted to ASCII text (.dta

297   format) using MSConvert (http://proteowizard.sourceforge.net/tools/msconvert.html) which

298   more precisely assigns the charge and parent mass values to an MS/MS spectrum. The data files

299   were then interrogated via target-decoy approach

300   (http://www.ncbi.nlm.nih.gov/pubmed/20013364) using MSGFPlus

301   (http://www.ncbi.nlm.nih.gov/pubmed/25358478) using a +/- 20 ppm parent mass tolerance,

302   partially tryptic digestion enzyme settings, and a variable posttranslational modification of

303   oxidized Methionine. All MS/MS search results for each dataset were collated into tab separated

304   ASCII text files listing the best scoring identification for each spectrum.

305   Collated search results were further combined into a single result file. These results were

306   imported into a Microsoft SQL Server database. Results were filtered to >1% FDR using an

307   MSGF+ supplied Q-Value that assesses reversed sequence decoy identifications for a given

308   MSGF score across each dataset. Using the protein references as a grouping term, unique

309   peptides belonging to each protein were counted, as were all peptide spectrum matches (PSMs)

310   belonging to all peptides for that protein (i.e. a protein level observation count value). PSM

311   observation counts reported for each sample that was analyzed. Cross-tabulation tables were

312   created to enumerate protein level PSM observations for each sample, allowing low-precision

313   quantitative comparisons to be made. Identified proteins were searched against dbCAN v5 (Yin

314   et al., 2012) using hmmer v3.1 (Finn et al., 2011). CAZy families were assigned based on cutoff

315   suggestions of the maintainers of dbCAN. We removed singletons and proteins not present in at

316   least 25% of samples prior to statistical analysis. Samples with less than 10 total protein counts

317   (n = 4) were removed from our dataset to yield 29 samples.

318

319   *2.9. Statistical analyses.*

320   After removing samples with low protein detection, we retained 29 samples for statistical

321   analyses. To identify hotspots vs. low-activity sediments, we examined the distribution of

322   aerobic metabolism rates in all 29 samples (Fig. S4). The distribution was approximately normal

323   with a minimum of 361.83, a mean of 810.49, and a maximum of 1472.86. We defined low-

324   activity sediments as those falling in the bottom quartile of the distribution (maximum rate of

325   aerobic metabolism: 619.45) and high activity samples as those falling in the top quartile of the

326   distribution (minimum rate of aerobic metabolism: 1033.66), yielding a sample size of 7 for each

327   set of samples. All statistical analyses were conducted using R software (https://www.r-

328   project.org/) and graphics were generated with either base packages or 'ggplot2.'

329   We used two approaches to determine differences in the composition of metabolites,

330   microbial phylogenies, metagenomic functional potential (i.e., all annotated genes), and

331   metaproteomes between hotspots and low-activity sediments. Metabolomes were analyzed as

332   present/absence data, and all other data types were analyzed as relative abundances. First, we

333   examined differences in full compositional profiles across groups using permutational

334   multivariate analysis of variance (PERMANOVA, 999 permutations, 'vegan' package) and

335   accounting for potential non-independence between samples within the same core by stratifiying

336   this analysis by depth (as per Graham et al., 2017b). Because metabolite data were in

337   presence/absence form, a Sorenson dissimilarity distance was constructed and used to compare

338   metabolite data. All other datasets were analyzed using Bray-Curtis dissimilarity to account for

339   differences in relative abundance.

340   Secondly, we used linear mixed effect models to investigate variation in specific

341   microbial attributes between hotspots and low-activity sediments. Following the convention of

342   Graham et al. (2017b), we included depth as a random effect in these models to account for

343   possible non-independence among sediments. A given microbial attribute was the dependent

344   variable and sediment type was the independent variable. Mixed models were compared to null

345   expectations (i.e., a model including only random effects) with analysis of variance (ANOVA) to

346   determine significance. For significant models ($P < 0.05$), R^2 values for microbial attributes

347   independently and for the entire mixed model (i.e., the effects of the attribute plus depth) were

348   determined with the 'r.squaredGLMM' function in the 'MuMIn' package (Barton, 2009).

349   Because few compounds differed across activity levels, P-values were not adjusted for multiple

350   comparisons in order to maximize the likelihood of detecting differences.

351   We selected specific attributes for analysis as follows: For metabolomic data, we grouped

352   peaks by their Van Krevlen assignment and compared the relative abundance of each Van

353   Krevlen class across activity groups (e.g., the relative abundance of amino sugars in hotspots vs.

354   low-activity sediments). To identify specific microbial phylogenic and functional groups of

355   interest, we employed the following procedure: (1) we ranked the relative abundance of each

356   assigned phylogeny (class level) or functional annotation (pfam, COG, and KEGG) within each

357   sample; (2) we compiled a master list containing the 25 most abundant phylogenies or functional

358   annotations in every sample; and (3) we determined the relative abundance of every unique

359   phylogeny or functional annotation in the master list within each sample. In this way, we

360   examined every taxon or metabolic pathway that was present in high abundance in at least one

361   sample. For metaproteomic data, we employed a similar pipeline but because the proteomic

362   dataset was smaller, we comprised our master list from any protein in the top 5% of relative

363   abundance in a given sample (equivalent to more than 10 proteins per sample).

364   Because (1) metagenomes did not vary strongly between hotspots and low-activity

365   sediments, (2) proteins are tightly coupled to function conceptually (i.e., they are proximate

366   catalysts of reactions), and (3) metabolites were dramatically different across activity levels; we

367   focused subsequent analyses only on metaproteomic and metabolomics data. We first

368   investigated the extent to which metaproteome structure corresponded to metabolome structure

369   in the full dataset (n = 29) by comparing dissimilarity in metabolite composition (Sorenson

370   dissimilarity) to differences in proteomic composition (Bray-Curtis dissimilarity, Mantel test

371   using Spearman correlation and stratifying by depth). We also examined the extent to which each

372   data type corresponded to changes in aerobic metabolism by fitting linear and quadratic mixed

373   effects models across the full dataset. As above, depth was included as a random effect in each

374   model. To reduce multidimensional metaproteomic and metabolomic data into vectors for model

375   construction, we extracted the first two principle components of variation within data type (PCA

376   analysis, 'prcomp'). PC1 and PC2 were predictors in the mixed effects models, and aerobic

377   metabolism was the response variable. Mixed models were compared to null expectations (i.e.,

378   models including only random effects) with ANOVA to determine significance. R^2 values were

379   determined with the 'r.squaredGLMM' function in the 'MuMIn' package. Since both PC1 and

380   PC2 from metabolomes were significantly related to aerobic metabolism, we also constructed a

381   model that included both PC1 and PC2 as predictors. Lastly, to examine additional explanatory

382   power that could be gained by incorporating bulk C as predictors along with metabolite

383   chemistry, we constructed a final model with PC1, PC2, and percent C. This model was

384   compared to the model with PC1 and PC2 only using ANOVA to determine if percent C

385   significantly improved explanatory power of aerobic metabolism.

386   Finally, because metabolomes were most distinguishing between hotspots and low-

387   activity sediments and corresponded to rates of aerobic metabolism, we concluded with set of

388   analyses with metabolomic data only. We deciphered specific metabolites that distinguished

389   hotspots from low-activity sediments using 'random forest' machine learning algorithm (Liaw

390   and Wiener, 2002, 'randomForest' package). Forests were constructed using metabolite peaks

391   that were assigned chemical formulae, removing singletons for computational limitations. For

392   each forest, 1000 trees were constructed with replacement, and error rates converged near zero

393   (Fig. S5). Peak importance and partial dependence in distinguishing high vs. low activity

394   samples were calculated with the 'imp' and 'PartialPlot' functions, respectively. Peaks that were

395   assigned a 'Mean Decrease in Accuracy' of greater than zero were considered to be

396   distinguishing metabolites. This approach yielded 55 peaks distinguishing low activity samples

397   and 272 peaks distinguishing high activity samples.

398   We also used metabolite transformations to infer biochemical processes associated with

399   aerobic metabolism in hotspots. We identified transformations of interest using the following

400   procedure: (1) we summed the relative abundance of each transformation across all samples (n =

401   29) and (2) we chose the transformations whose abundance was in the top 20% of all

402   transformations (18 out of 92, mean relative abundance: 1.6% to 14.5%). By doing so, we

403   analyzed transformations that occurred most frequently in our dataset, irrespective of their

404   occurrence within individual samples.

405   We then compared the relative abundance of specific transformations between hotspots

406   and low-activity sediments using linear mixed effect models using the same procedure as for

407   abundant microbial phyologenies, metabolic pathways, expressed proteins, and metabolites

408   (described above). Because many abundant transformations in hotspots seemed to contain

409   nitrogen (N) while transformations in low-activity sediments did not, we also examined the role

410   in nitrogenous compounds in biochemical transformations in hotspots. We separated

411   transformations into those containing N and N-free transformations (Table S3 and S4) and

412   determined the relative abundance of transformations in each sample that were either nitrogenous

413   or N-free. We then compared the relative abundance of nitrogenous and N-free compounds

414   between hotspots and low-activity sediments using mixed effects models. Because the

415   distribution of transformations within nitrogenous and N-free categories was highly non-

416   Gaussian, we applied a Box-Cox transformation to each data type ('boxCox' function in 'car'

417   package, Sakia, 1992), and subsequently constructed linear mixed effects models. We further

418   separated amino-acid nitrogenous transformations from non-amino acid nitrogenous

419   transformations (hereafter 'complex N', Table S5 and S6), applied a Box-Cox transformation,

420   and constructed linear mixed effects models with these data.

421

422   **3. Results.**

423   *3.1. Multi 'Omic Differences across Rates of Aerobic Metabolism*

424   Microbiome structure, functional potential, and protein expression showed limited

425   differences between hotspots vs. low-activity sediments. No significant difference was observed

426   in the composition of microbiome phylogenies ($P = 0.57$, Fig. 1a), metagenomic annotations ($P =$

427   0.69, Fig. 1b), and metaproteomes ($P = 0.91$, Fig. 1c) between hotspots and low-activity

428   sediments (PERMANOVA). As well, major clades, pathways, and proteins were similar among

429   sediments (Fig. 1).

430   Metabolome composition, however, differed between hotspots and low-activity samples

431   (P = 0.01, R^2 = 0.28, Fig. 1d, PERMANOVA). When grouped into major compound classes,

432   hotspots contained more amino sugar- and protein-like metabolites (P < 0.05, Fig. 1d, mixed

433   effects). Metabolite pool composition was uncorrelated to proteome structure (P = 0.62, Fig. S6,

434   Mantel test across all samples).

435   Finally, when considering aerobic metabolism as a continuous variable, metabolome

436   composition was tightly correlated to aerobic metabolism. The first two principle coordinates of

437   metabolite pool composition had significant independent relationships with aerobic metabolism

438   and together explained 67% of variation in aerobic metabolism (mixed effects, P (PC1, quad.) =

439   0.0006 & P (PC2, linear) = 0.01, P (combined, linear) << 0.0001, Fig. 2a, Fig. S7). Statistical

440   models including both bulk C and metabolite composition were not significantly different from

441   models including metabolite composition alone (R^2 0.73 vs. 0.67, P = 1). Metaproteome

442   composition was uncorrelated to aerobic metabolism despite representing the proximal catalysts

443   of metabolic processes (mixed effects, P (PC1) = 0.29 & P (PC2) = 0.53, Fig. 2b).

444

445   *3.2. Distinguishing Metabolite Chemistry and Transformations*

446   Because hotspots were discriminated from low-activity sediments only in the

447   metabolome, we examined metabolite pools to identify compounds and infer processes that

448   distinguished hotspots from low-activity sediments. Hotspots were characterized by high

449   molecular weight (P < 0.0001, Fig. 3a), chemically diverse (Fig. 3b) compounds. In particular,

450   nitrogenous classes of compounds (i.e., amino sugars and proteins) were present in metabolites

451   that described hotpots and absent from metabolites characterizing low activity sediments (Fig.

452   3b).

453   Hotspots also exhibited a more even distribution of abundant biochemical

454   transformations, indicating greater diversity of biogeochemical processes in these sediments

455   relative to low-activity sediments (Fig. 4a). These transformations were inferred by comparing

456   differences between peaks in FT-ICR-MS data to a database of known biochemical

457   transformations (see section 2.6). Further, transformations involving nitrogenous compounds (P

458    $= 0.03$ $R^2 = 0.26$, Table S3), particularly those involving complex N (P $= 0.04$ $R^2 = 0.20$, Fig. 4b,

459   Table S6)), were more prevalent in hotspots.

460

461   **4. Discussion.**

462   Our multi 'omics investigation of microbiome structure and function in hyporheic zone

463   hotspots highlights the importance of vegetation in driving local-scale ($<200m^2$) aerobic

464   metabolism in the subsurface. Pronounced spatial heterogeneity in metabolism across our

465   relatively small spatial domain (~175 x 10m) is inconsistent with representations of

466   biogeochemical processes within ecosystem models that often aggregate environmental

467   properties across similarly sized domains, and suggests a need for finer scale representation of

468   processes in these models. Our research supports previous observations of relationships between

469   riparian vegetation and hyporheic zone hotspots due to associated carbon and nutrient inputs

470   (Harms and Grimm, 2008; McClain et al., 2003; Schade et al., 2001). For example, Kuglerova et

471   al. (2014) demonstrated that increased vegetation growth corresponded to enhanced

472   biogeochemical cycling in areas of the hyporheic zone experiencing maximal groundwater-

473   surface water mixing. In our system, hotspots were disproportionately distributed within

474   sediments underlying vegetation and exhibited up to 4 times the rate of aerobic metabolism in

475   low-activity sediments despite a small sampling domain (Fig. S4).

476   Contrary to our hypothesis that microbiome composition (metagenomics) and expression

477   (metaproteomics) would be shifted towards carbohydrate metabolism in hotspots, our results

478   support a predominant role for phenotypic plasticity within sediment microbiomes. Phenotypic

479   plasticity, whereby an organism encodes multiple metabolic pathways and adjusts the expression

480   of each depending on environmental conditions, is common in free-living microbes and

481   manifests as different metabolisms occurring in samples with the same genomic composition.

482   Microbiome phylogeny and functional potential did not vary with the level of aerobic respiration

483   in our sediments. While Hartman *et al.* (2017) demonstrated a consistent metagenomic shift from

484   aromatic to carbohydrate metabolism with increased carbon turnover in global soils, we observed

485   no such relationship in our sediments. A key difference between Hartman *et al.* (2017) and the

486   present study is that Hartman *et al.* demonstrated decreased nutrient uptake with increased

487   activity. In the present study, decreased nutrient uptake would correspond to fewer nitrogenous

488   biochemical transformations, whereas we observed increasing activity of biochemical pathways

489   involving nitrogen in hotspots vs. low-activity sediments. The lack of microbiome change in our

490   study may therefore be constrained by N-limitation. For instance, if microbiomes in our

491   sediments are always under strong selection for N-harvesting metabolisms, they would be

492   structured to contain organisms with the ability to metabolize organic N (Craine et al., 2007;

493   Moorhead and Sinsabaugh, 2006), regardless of the magnitude of available N.

494   Interestingly, while one would expect protein expression to correlate with changes in

495   activity, we saw no such effect in our metaproteomic data. The long residence time of enzymes

496   compared to hydrologic mixing may decouple expression from function in dynamic

497   environments such as the hyporheic zone. Hydrologic exchange in the hyporheic zone occurs on

498   relatively short time scales (commonly minutes to days), as well as longer seasonal exchanges,

499   and creates fleeting periods of nutrient availability (Cardenas et al., 2008; Fritz and Arntzen,

500   2007; Sawyer and Cardenas, 2009; Zarnetske et al., 2011). Recent work in soils has shown that

501   protein decay rates vary widely across enzymes and that some enzymes can persist more than 12

502   weeks in soils (Schimel et al., 2017). Assuming a similar magnitude of decay in hyporheic zone

503   sediments would generate a disconnect between protein expression and resource availability that

504   may ultimately disassociate enzyme pool composition from respiration rates, leading to the lack

505   of relationship between metaproteome composition and aerobic metabolism observed here.

506   Our results indicate that improved resolution into sediment metabolomes provides greater

507   insight into sediment function than bulk C content at a given point in time. While there is a long

508   history of constraining biogeochemical rates with standing resource pools, our work indicates

509   that bulk C alone was an insufficient predictor of aerobic respiration (Fig. S8). Metabolite

510   chemistry explained 67% of variation in aerobic metabolism (in comparison to 42% by bulk C

511   pools, Fig. S8), and including bulk C content as a predictor in addition to metabolome

512   composition did not improve the explanatory power of our statistical models. In particular,

513   nitrogenous metabolites were associated with enhanced metabolism. We therefore suggest that

514   metabolome composition can explain aerobic metabolism better than bulk C stocks in some

515   systems and subsequently that new process-based model structures need to account for multiple

516   C pools with various organic N content. For instance, current generation models incorporate

517   mechanisms reflecting that certain C molecules (e.g., glucose) can enter microbial cells by

518   passing directly through their cellular membranes, while larger molecules require secreted

519   extracellular enzymes to break them down prior to microbial uptake (Wang et al., 2013; Wieder

520   et al., 2014). Extending these new frameworks to further parse C chemistry by organic N content

521   and associated metabolic pathways could advance the performance of these models.

522   Microbiomes associated with hyporheic zone hotspots metabolized a broader range of

523   resources compared to microbiomes in low-activity sediments. Enhanced biogeochemical

524   cycling can be achieved through microorganisms using different portions of resource pools

525   (termed 'resource partitioning' or 'niche complementarity') in which diverse microorganisms use

526   different portions of resource pools (Cardinale, 2011; Loreau and Hector, 2001; Schoener, 1974).

527   Consistent with this mechanism, we show a divergence in active metabolic pathways (inferred

528   from biochemical transformations) in hotspots compared to low-activity sediments. Thus, despite

529   similar microbiome genomic content, hotspots seem to result from the expansion of realized

530   niches of extant microbiomes. In this case, increased biogeochemical function arises through

531   phenotypic plasticity.

532   Hotspots contained diverse metabolites, were distinguished from low-activity sediments

533   by protein- and amino sugar- like metabolites, and exhibited higher instances of biochemical

534   transformations involving organic N. It has been widely demonstrated that N availability can

535   limit microbial activity (Treseder, 2008), resulting in slower decomposition and ecosystem

536   organic matter processing (Averill and Waring, 2017; Weintraub and Schimel, 2003; Zhang et

537   al., 2008); and previous work in this system has suggested a coupling of C and N cycles (Stegen

538   et al., 2018). An excess of inorganic N relative to other N sources has also been demonstrated to

539   shift microbial metabolism by suppressing oxidative enzyme synthesis (Edwards et al., 2011;

540   Jian et al., 2016) and by changing the ratios of synthesized enzymes that degrade recalcitrant vs.

541   labile organic matter (Moorhead and Sinsabaugh, 2006). Similarly our analysis of metabolite

542   transformations supports different metabolic strategies among hotspot vs. low-activity

543   microbiomes as well as a role for organic N in particular as a driver of aerobic metabolism in

544   hotspots.

545   While C:N ratios do not reflect obvious N limitation in our system (means: 6.55 (hotspot)

546 and 6.19 (low-activity)), these ratios can misrepresent chemical conditions experienced by

547 microbiomes due to N absorption to soil matrices and by aggregation processes that physically

548 separate N from microorganisms (Lützow et al., 2006; Sollins et al., 1996). For instance,

549 Darrouzet-Nardi and Weintraub (2014) demonstrated that bulk methods of C and N

550 determination such as those used here may overestimate N availability by 5-fold. As such,

551 organic N may play a critical role in our system despite ratios of C:N in bulk sediments.

552   Moorhead and Sinsabaugh (2006) proposed a concept known as 'microbial nitrogen

553 mining' in which microorganisms in environments with limited availability of labile N

554 metabolize C to access organic N (Craine et al., 2007; Moorhead and Sinsabaugh, 2006).

555 Microbial N mining should result in the preferential decomposition of organic N, and our results

556 indicate that this process may contribute to high respiration rates in hyporheic zone hotspots.

557 Consistent with N mining, we observed biochemical pathways involving nitrogenous

558 compounds, and complex N in particular within hotspots, supporting previous observations that

559 organic N increases the decomposition of organic matter (reviewed in Averill and Waring, 2017;

560 Hu et al., 2001; Zhang et al., 2008). The metabolism of complex nitrogenous organic compounds

561 specifically suggests that the breakdown of more chemically-complex organic material may be

562 stimulated to facilitate microbial access to nitrogen and that more available labile C in vegetated

563 sediments provides additional energy necessary to metabolize more chemically-complex

564 nitrogenous molecules.

565   Based on our results, we propose a new conceptualization of hyporheic zone organic

566 matter transformations in which greater resolution into C metabolites and associated metabolic

567 pathways—beyond bulk C stocks and/or microbiome structure—is critical for predictive

568   hydrobiogeochemical models (Fig. 5). Phenotypic plasticity suggests (1) an ability for

569   microbiomes to rapidly acclimate to environmental conditions, regardless of their underlying

570   genomic content, and (2) that there may be limited contributions of metagenomic information to

571   functional predictions in dynamic systems. Because compositional shifts in microbiomes are

572   often on the order of days to months or longer (Balser and Firestone, 2005; Graham et al., 2016a;

573   Poretsky et al., 2014; Waldrop and Firestone, 2006), the ability of microorganisms to adjust

574   metabolic function to suit prevailing conditions without associated species turnover denotes that

575   the timescale of microbiome response is not limited to these longer timescales and instead that

576   microbial responses in some systems may be more tightly constrained by RNA transcription and

577   translation (~minutes or less, Moran et al., 2013).

578   Further, we suggest that broader metabolic activity in biogeochemical hotspots stimulates

579   the production and consumption of diverse metabolites which alter the composition of future

580   resource pools, and therefore that understanding subsequent feedbacks between metabolite

581   consumption and production is vital for predictive biogeochemical models. For example, as

582   metabolism proceeds through time, future metabolic rates are dependent on the resources (i.e.,

583   metabolites) generated by these pathways. Metabolism of an expanded suite of resources through

584   broader realized niche space within biogeochemical hotspots may therefore fundamentally

585   change the subsequent metabolite and resource profiles (Fig. 5). As hotspots and hot moments

586   occur through time and space, resource pools progressively change in ways that are dependent on

587   microbial transformations of prior resource pools, and knowledge about the specific metabolic

588   pathways that generate propagating changes as well as their rates and limitations is imperative

589   for improving biogeochemical predictions. Our results also demonstrate organic N in particular

590   may be involved these alternative pathways, and thus, that nutrient limitations are important

591   considerations in constraining rates within predictive models, as has been recently explored by

592   Wieder et al (2015b). We further extended this conceptualization to propose that organic N

593   specifically should be considered as a possible regulatory factor in process-based ecosystem

594   models.

595   The fate of organic carbon stored in soils and sediments, particularly at terrestrial-aquatic

596   interfaces (Battin et al., 2009; Boulton et al., 1998; Cole et al., 2007; Marín-Spiotta et al., 2014;

597   Regnier et al., 2013), is responsible for large amounts of uncertainty in predictions of future

598   global biogeochemistry (Luo et al., 2016; Todd-Brown et al., 2013). Here, we provide insight

599   into the molecular mechanisms generating hotspots of elevated aerobic metabolism in the

600   hyporheic zone. While microbiome structure and protein expression did not vary across levels of

601   aerobic metabolism, we found that metabolite chemistry and diverse, N-related biochemical

602   pathways were associated with hyporheic zone hotspots. We posit that microbiome phenotypic

603   plasticity can enable microbiomes with similar structure to expand their realized niche in

604   response to changing environments and rapidly increase function in favorable environments.

605   Because of fleeting environmental changes within hyporheic zones, we hypothesize that

606   hyporheic zone microbiomes may exhibit more phenotypic plasticity than more stable

607   ecosystems, meriting further investigation as we explore spatiotemporal dynamics across

608   multiple systems (Fodelianakis et al., 2017). As we search for consensus on the importance of

609   various environmental factors in predicting future biogeochemical rates (Graham et al., 2016b;

610   Graham et al., 2014; Luo et al., 2016; Wieder et al., 2017), a spatially-explicit understanding of

611   the mechanisms regulating organic matter transformations in areas with elevated biogeochemical

612   rates is essential for improving the conceptualization and parameterization of ecosystem models.

613   We propose that understanding and constraining the rates of specific metabolic pathways that

614   utilize discrete portions of resource pools is a critical consideration when advancing carbon cycle

615   complexity in these models.

616

625
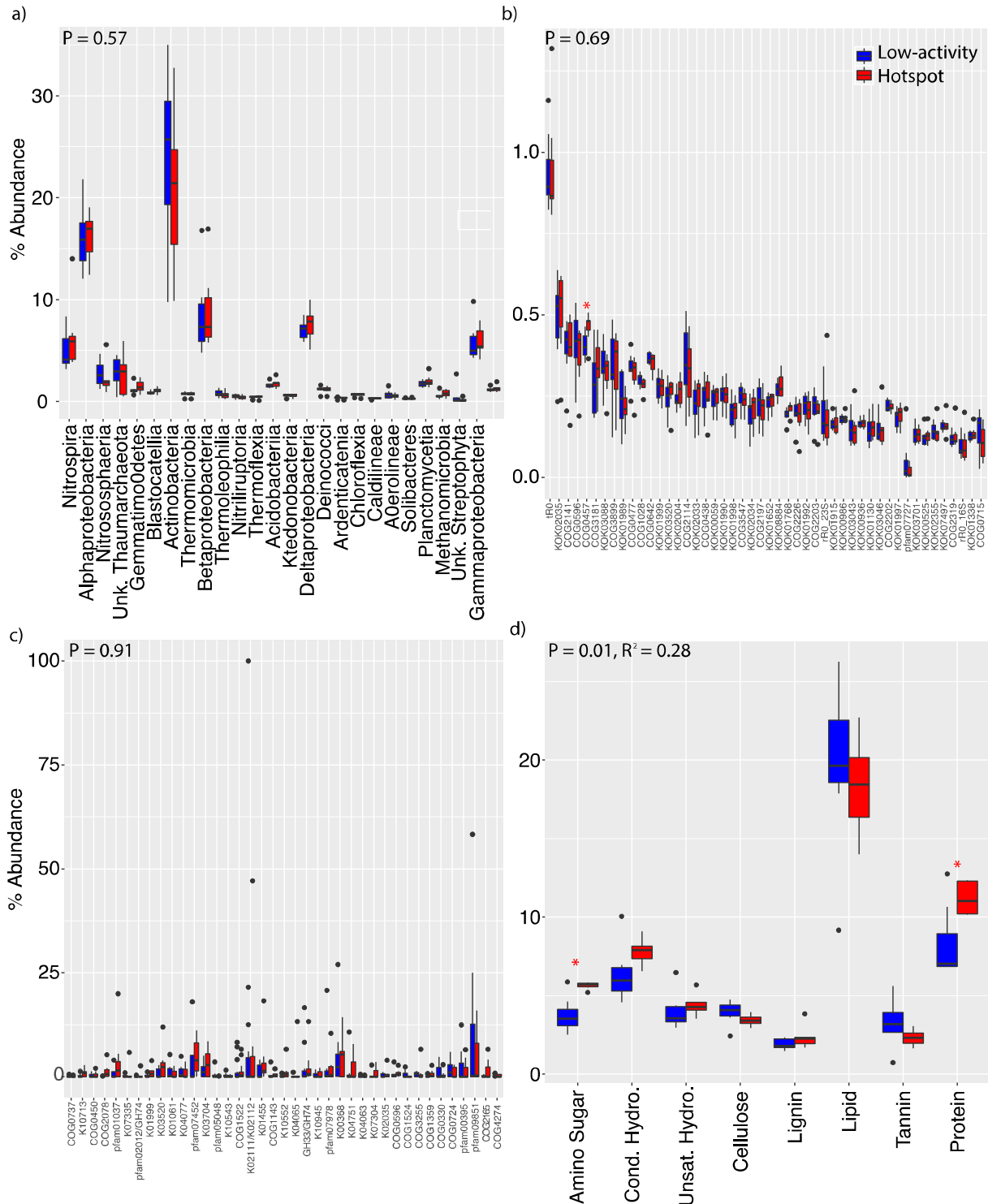
626   **Figures.**

627

628 **Fig. 1. Multi 'Omic Differences in Hotspots vs. Low-activity Sediments.** (a-d) show the most

629 abundant classifications only for visual simplicity, but P-values in the upper left-hand corner of

630 each panel are derived from all data. P-values are derived from PERMANOVA with

631 stratification by depth. R^2 values are provided for significant P-values. (a) shows abundant

632 microorganisms (grouped at the class level), (b) shows abundant metagenomics annotations, (c)

633 shows abundant metaproteomic identifications, and (d) shows metabolomics data grouped by

634 compound class. Asterisks denote significant differences between hotspots and low-activity

635 sediments, via mixed models with depth as a random effect ($P < 0.05$).
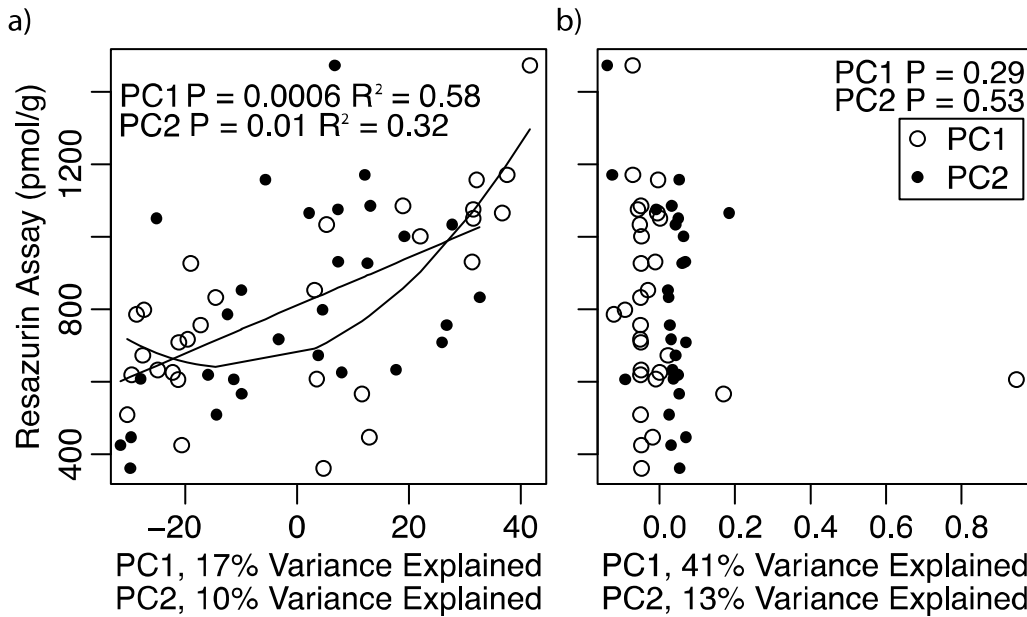
636

637

638

Fig. 2. Relationships of Metabolomes and Metaproteomes with Aerobic Metabolism. The

first two principle components were extracted from metabolomics and metaproteome data.

Correlations between each component and aerobic metabolism were determined using linear and

quadratic mixed models that included depth as a random effects. Regression lines are shown for

the best model; only significant models are shown. (a) Metabolomic data were strongly

correlated with aerobic metabolism, while (b) metaproteomic data were uncorrelated.
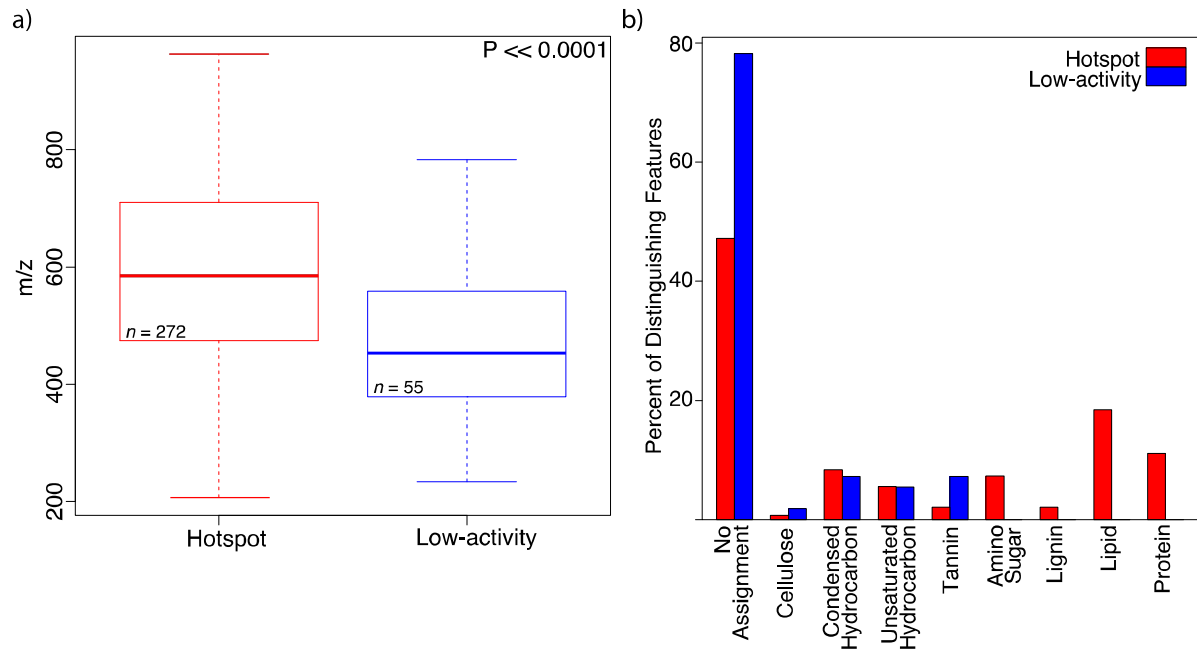
645

646

Fig. 3. Metabolites Distinguishing Hotspots from Low-Activity Sediments. (a) The molecular weight of distinguishing metabolites was significantly higher in hotspots than low-activity sediments. A boxplot of molecular weights are shown, with the center line indicating the mean and the hinges of each box representing the values at the 25th and 75th percentiles. The whiskers represent the range of the data, calculated using default settings in R. P-value is derived from a one-sided Mann-Whitney U test. (b) shows the distribution of distinguishing metabolites in hotspots vs. low-activity sediments. Compounds are grouped by molecular class and displayed as a percent of distinguishing metabolites in each class.
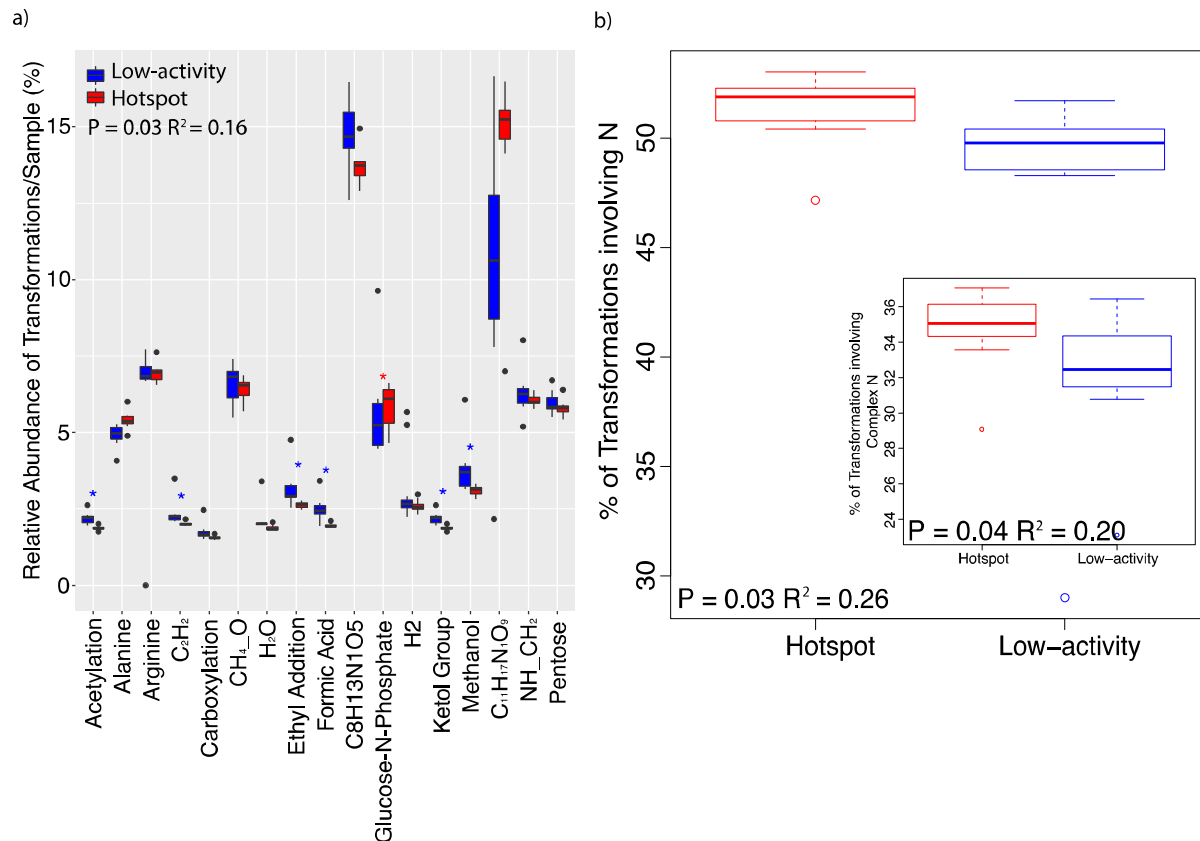
658

Fig. 4. Differences in Biochemical Transformations between Hotspots and Low-activity

Sediments. (a) shows the most abundant transformations only for visual simplicity, but the P-value in the upper left-hand corner is derived from all data. Asterisks denote significant differences between hotspots and low-activity sediments, via mixed models with depth as a random effect (P < 0.05). (b) shows a boxplot of the percent of transformations involving N across hotspots and low-activity sediments. The inset shows the same analysis using only transformations involving 'complex N'. Lists of the specific transformations included in each analysis are shown in Tables S3-S6. For each boxplot, with the center line indicating the mean and the hinges of each box representing the values at the 25th and 75th percentiles. The whiskers represent the range of the data, calculated using default settings in R. P-values and R^2 are calculated using mixed models with depth as a random effect. Due to non-normality in the

670   distribution of transformations, a Box-Cox transformation was applied prior to model
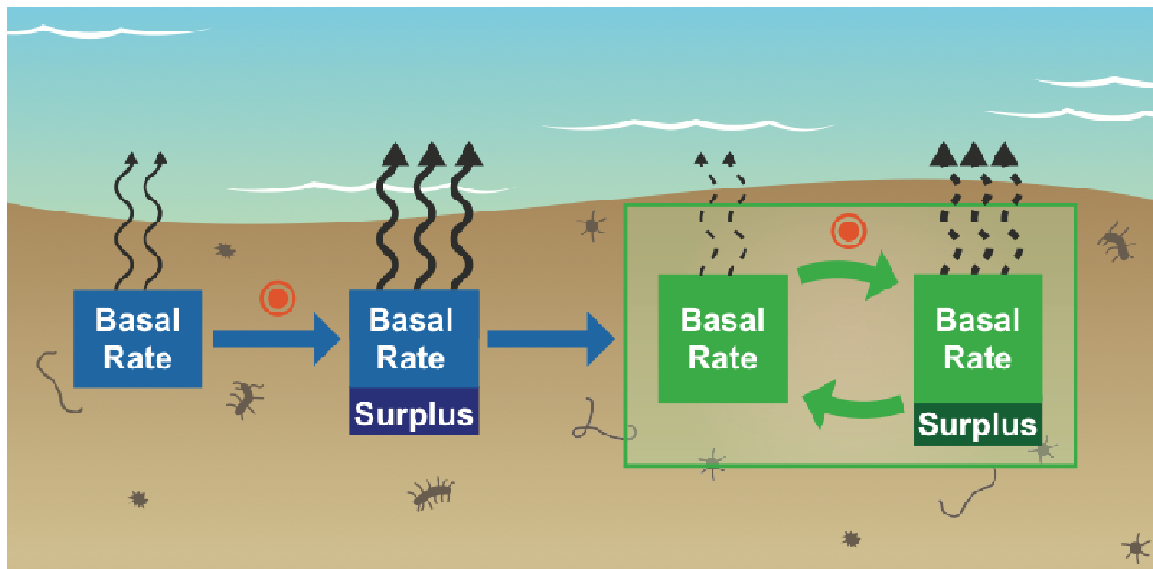
671   construction.

672

673

Fig. 5. Conceptualization of a Role for Metabolic Pathways in CO_2 Flux Predictions. We propose that greater resolution into C metabolites and associated metabolic pathways—beyond sediment bulk C and/or microbiome structure—is vital for predictive hydrobiogeochemical models. Broader metabolic activity in biogeochemical hotspots stimulates the production and consumption of diverse metabolites, in particular nitrogenous compounds. Therefore, there is a need to incorporate subsequent feedbacks between metabolite consumption and production into predictive biogeochemical models. Orange bull's eyes represent the occurrence of a hotspot or hot moment. Basal rate is the baseline aerobic metabolism of sediments. Surplus metabolism indicates the increase in aerobic metabolism associated with hotspots and includes stimulated organic N respiration. Arrows denote CO_2 flux, where the number and thickness of arrow denotes the relative size of the flux. Blue boxes indicate the initial condition of sediments and the first occurrence of a hotspot or hot moment. Green boxes show an ongoing feedback loop in which the basal rate of a microbiome is continuously influenced by metabolite production and consumption.

688 **References.**

689 Aebersold R, Mann M. Mass spectrometry-based proteomics. Nature 2003; 422: 198-207.

690 Allison SD, Wallenstein MD, Bradford MA. Soil-carbon response to warming dependent on

691   microbial physiology. Nature Geoscience 2010; 3: 336-340.

692 Arntzen EV, Geist DR, Dresel PE. Effects of fluctuating river flow on groundwater/surface water

693   mixing in the hyporheic zone of a regulated, large cobble bed river. River Research and

694   Applications 2006; 22: 937-946.

695 Averill C, Waring B. Nitrogen limitation of decomposition and decay: How can it occur? Global

696   change biology 2017.

697 Bailey VL, Smith A, Tfaily M, Fansler SJ, Bond-Lamberty B. Differences in soluble organic

698   carbon chemistry in pore waters sampled from different pore size domains. Soil Biology

699   and Biochemistry 2017; 107: 133-143.

700 Balser TC, Firestone MK. Linking microbial community composition and soil processes in a

701   California annual grassland and mixed-conifer forest. Biogeochemistry 2005; 73: 395-

702   415.

703 Barton K. MuMIn: multi-model inference. R package version 1. 0. 0. http://r-forge. r-project.

704   org/projects/mumin/ 2009.

705 Battin TJ, Luyssaert S, Kaplan LA, Aufdenkampe AK, Richter A, Tranvik LJ. The boundless

706   carbon cycle. Nature Geoscience 2009; 2: 598-600.

707 Boulton AJ, Findlay S, Marmonier P, Stanley EH, Valett HM. The functional significance of the

708   hyporheic zone in streams and rivers. Annual Review of Ecology and Systematics 1998;

709   29: 59-81.

710   Breitling R, Ritchie S, Goodenowe D, Stewart ML, Barrett MP. Ab initio prediction of metabolic

711   networks using Fourier transform mass spectrometry data. Metabolomics 2006; 2: 155-

712   164.

713   Buchkowski RW, Bradford MA, Grandy AS, Schmitz OJ, Wieder WR. Applying population and

714   community ecology theory to advance understanding of belowground biogeochemistry.

715   Ecology letters 2017; 20: 231-245.

716   Burd AB, Frey S, Cabre A, Ito T, Levine NM, Lønborg C, et al. Terrestrial and marine

717   perspectives on modeling organic matter degradation pathways. Global change biology

718   2016; 22: 121-136.

719   Cardenas MB, Wilson JL, Haggerty R. Residence time of bedform-driven hyporheic exchange.

720   Advances in Water Resources 2008; 31: 1382-1386.

721   Cardinale BJ. Biodiversity improves water quality through niche partitioning. Nature 2011; 472:

722   86-89.

723   Cole JJ, Prairie YT, Caraco NF, McDowell WH, Tranvik LJ, Striegl RG, et al. Plumbing the

724   global carbon cycle: integrating inland waters into the terrestrial carbon budget.

725   Ecosystems 2007; 10: 172-185.

726   Craine JM, Morrow C, Fierer N. Microbial nitrogen limitation increases decomposition. Ecology

727   2007; 88: 2105-2113.

728   Darrouzet-Nardi A, Weintraub MN. Evidence for spatially inaccessible labile N from a

729   comparison of soil core extractions and soil pore water lysimetry. Soil Biology and

730   Biochemistry 2014; 73: 22-32.

731   Edwards IP, Zak DR, Kellner H, Eisenlord SD, Pregitzer KS. Simulated atmospheric N

732   deposition alters fungal community composition and suppresses ligninolytic gene

733   expression in a northern hardwood forest. PloS one 2011; 6: e20421.

734   Finn RD, Clements J, Eddy SR. HMMER web server: interactive sequence similarity searching.

735   Nucleic acids research 2011; 39: W29-W37.

736   Fodelianakis S, Moustakas A, Papageorgiou N, Manoli O, Tsikopoulou I, Michoud G, et al.

737   Modified niche optima and breadths explain the historical contingency of bacterial

738   community responses to eutrophication in coastal sediments. Molecular ecology 2017;

739   26: 2006-2018.

740   Fritz BG, Arntzen EV. Effect of rapidly changing river stage on uranium flux through the

741   hyporheic zone. Ground Water 2007; 45: 753-760.

742   Gabor RS, Baker A, McKnight DM, Miller MP. Fluorescence indices and their interpretation.

743   Aquatic Organic Matter Fluorescence 2014; 303.

744   Gomez-Velez JD, Harvey JW, Cardenas MB, Kiel B. Denitrification in the Mississippi River

745   network controlled by flow through river bedforms. Nature Geoscience 2015; 8: 941-945.

746   Graham EB, Crump AR, Resch CT, Fansler S, Arntzen E, Kennedy DW, et al. Coupling

747   spatiotemporal community assembly processes to changes in microbial metabolism.

748   Frontiers in Microbiology 2016a; 7.

749   Graham EB, Crump AR, Resch CT, Fansler S, Arntzen E, Kennedy DW, et al. Deterministic

750   influences exceed dispersal effects on hydrologically‐connected microbiomes.

751   Environmental Microbiology 2017a; 19: 1552-1567.

752   Graham EB, Knelman JE, Schindlbacher A, Siciliano S, Breulmann M, Yannarell A, et al.

753   Microbes as engines of ecosystem function: when does community structure enhance

754   predictions of ecosystem processes? Frontiers in microbiology 2016b; 7.

755   Graham EB, Tfaily MM, Crump AR, Goldman AE, Bramer L, Arntzen E, et al. Carbon inputs

756   from riparian vegetation limit oxidation of physically-bound organic carbon via

757   biochemical and thermodynamic processes. Journal of Geophysical Research:

758   Biogeosciences 2017b.

759   Graham EB, Wieder WR, Leff JW, Weintraub SR, Townsend AR, Cleveland CC, et al. Do we

760   need to understand microbial communities to predict ecosystem function? A comparison

761   of statistical models of nitrogen cycling processes. Soil Biology and Biochemistry 2014;

762   68: 279-282.

763   Haggerty R, Martí E, Argerich A, Von Schiller D, Grimm NB. Resazurin as a "smart" tracer for

764   quantifying metabolically active transient storage in stream ecosystems. Journal of

765   Geophysical Research: Biogeosciences 2009; 114.

766   Harms TK, Grimm NB. Hot spots and hot moments of carbon and nitrogen dynamics in a

767   semiarid riparian zone. Journal of Geophysical Research: Biogeosciences 2008; 113.

768   Hartman WH, Ye R, Horwath WR, Tringe SG. A genomic perspective on stoichiometric

769   regulation of soil carbon cycling. The ISME journal 2017; 11: 2652.

770   Hu S, Chapin III F, Firestone M, Field C, Chiariello N. Nitrogen limitation of microbial

771   decomposition in a grassland under elevated CO_2. Nature 2001; 409: 188.

772   Huizenga A, Bailey RT, Gates TK. Stream-aquifer and in-stream processes affecting nitrogen

773   along a major river and contributing tributary. Journal of Contaminant Hydrology 2017;

774   199: 24-35.

775   Huntemann M, Ivanova NN, Mavromatis K, Tripp HJ, Paez-Espino D, Palaniappan K, et al. The

776   standard operating procedure of the DOE-JGI Microbial Genome Annotation Pipeline

777   (MGAP v. 4). Standards in genomic sciences 2015; 10: 86.

778   Jian S, Li J, Chen J, Wang G, Mayes MA, Dzantor KE, et al. Soil extracellular enzyme activities,

779   soil carbon and nitrogen storage under nitrogen fertilization: A meta-analysis. Soil

780   Biology and Biochemistry 2016; 101: 32-43.

781   Kim S, Kramer RW, Hatcher PG. Graphical method for analysis of ultrahigh-resolution

782   broadband mass spectra of natural organic matter, the van Krevelen diagram. Analytical

783   Chemistry 2003; 75: 5336-5344.

784   Koch BP, Witt M, Engbrodt R, Dittmar T, Kattner G. Molecular formulae of marine and

785   terrigenous dissolved organic matter detected by electrospray ionization Fourier

786   transform ion cyclotron resonance mass spectrometry. Geochimica et Cosmochimica

787   Acta 2005; 69: 3299-3308.

788   Krause S, Lewandowski J, Grimm NB, Hannah DM, Pinay G, McDonald K, et al.

789   Ecohydrological interfaces as hotspots of ecosystem processes. Water Resources

790   Research 2017.

791   Kuglerová L, Jansson R, Ågren A, Laudon H, Malm-Renöfält B. Groundwater discharge creates

792   hotspots of riparian plant species richness in a boreal forest stream network. Ecology

793   2014; 95: 715-725.

794   Kujawinski EB, Behn MD. Automated analysis of electrospray ionization Fourier transform ion

795   cyclotron resonance mass spectra of natural organic matter. Analytical Chemistry 2006;

796   78: 4363-4373.

797   Li D, Luo R, Liu C-M, Leung C-M, Ting H-F, Sadakane K, et al. MEGAHIT v1. 0: A fast and

798   scalable metagenome assembler driven by advanced methodologies and community

799   practices. Methods 2016; 102: 3-11.

800   Liaw A, Wiener M. Classification and regression by randomForest. R news 2002; 2: 18-22.

801   Lin X, McKinley J, Resch CT, Kaluzny R, Lauber CL, Fredrickson J, et al. Spatial and temporal

802   dynamics of the microbial community in the Hanford unconfined aquifer. The ISME

803   Journal 2012; 6: 1665-1676.

804   Liski J, Palosuo T, Peltoniemi M, Sievänen R. Carbon and decomposition model Yasso for forest

805   soils. Ecological Modelling 2005; 189: 168-182.

806   Loreau M, Hector A. Partitioning selection and complementarity in biodiversity experiments.

807   Nature 2001; 412: 72-76.

808   Lotspeich FB, Reid BH. Tri-tube freeze-core procedure for sampling stream gravels. The

809   Progressive Fish-Culturist 1980; 42: 96-99.

810   Luo Y, Ahlström A, Allison SD, Batjes NH, Brovkin V, Carvalhais N, et al. Toward more

811   realistic projections of soil carbon dynamics by Earth system models. Global

812   Biogeochemical Cycles 2016; 30: 40-56.

813   Lützow Mv, Kögel-Knabner I, Ekschmitt K, Matzner E, Guggenberger G, Marschner B, et al.

814   Stabilization of organic matter in temperate soils: mechanisms and their relevance under

815   different soil conditions–a review. European Journal of Soil Science 2006; 57: 426-445.

816   Marín-Spiotta E, Gruley K, Crawford J, Atkinson E, Miesel J, Greene S, et al. Paradigm shifts in

817   soil organic matter research affect interpretations of aquatic carbon cycling: transcending

818   disciplinary and ecosystem boundaries. Biogeochemistry 2014; 117: 279-297.

819   Markley JL, Brüschweiler R, Edison AS, Eghbalnia HR, Powers R, Raftery D, et al. The future

820   of NMR-based metabolomics. Current opinion in biotechnology 2017; 43: 34-40.

821   McClain ME, Boyer EW, Dent CL, Gergel SE, Grimm NB, Groffman PM, et al. Biogeochemical

822   hot spots and hot moments at the interface of terrestrial and aquatic ecosystems.

823   Ecosystems 2003; 6: 301-312.

824   Minor EC, Steinbring CJ, Longnecker K, Kujawinski EB. Characterization of dissolved organic

825   matter in Lake Superior and its watershed using ultrahigh resolution mass spectrometry.

826   Organic Geochemistry 2012; 43: 1-11.

827   Moorhead DL, Sinsabaugh RL. A theoretical model of litter decay and microbial interaction.

828   Ecological Monographs 2006; 76: 151-174.

829   Moran MA, Satinsky B, Gifford SM, Luo H, Rivers A, Chan L-K, et al. Sizing up

830   metatranscriptomics. The ISME journal 2013; 7: 237-243.

831   Moser DP, Fredrickson JK, Geist DR, Arntzen EV, Peacock AD, Li S-MW, et al.

832   Biogeochemical processes and microbial characteristics across groundwater-surface

833   water boundaries of the Hanford Reach of the Columbia River. Environmental Science &

834   Technology 2003; 37: 5127-5134.

835   Naegeli MW, Uehlinger U. Contribution of the hyporheic zone to ecosystem metabolism in a

836   prealpine gravel-bed-river. Journal of the North American Benthological Society 1997;

837   16: 794-804.

838   Nicora CD, Burnum-Johnson KE, Nakayasu ES, Casey CP, III RAW, Chowdhury TR, et al. The

839   MPLEx Protocol for Multi-omic Analyses of Soil Samples. Jove in press.

840   Peterson RE, Connelly MP. Water movement in the zone of interaction between groundwater

841   and the Columbia River, Hanford site, Washington. Journal of Hydraulic Research 2004;

842   42: 53-58.

843   Poretsky R, Rodriguez-R LM, Luo C, Tsementzi D, Konstantinidis KT. Strengths and limitations

844   of 16S rRNA gene amplicon sequencing in revealing temporal microbial community

845   dynamics. PLoS One 2014; 9: e93827.

846   Regnier P, Friedlingstein P, Ciais P, Mackenzie FT, Gruber N, Janssens IA, et al. Anthropogenic

847   perturbation of the carbon fluxes from land to ocean. Nature geoscience 2013; 6: 597-

848   607.

849   Rocca JD, Hall EK, Lennon JT, Evans SE, Waldrop MP, Cotner JB, et al. Relationships between

850   protein-encoding gene abundance and corresponding process are commonly assumed yet

851   rarely observed. The ISME journal 2015; 9: 1693-1699.

852   Rood K, Church M. Modified freeze-core technique for sampling the permanently wetted

853   streambed. North American Journal of Fisheries Management 1994; 14: 852-861.

854   Sakia R. The Box-Cox transformation technique: a review. The statistician 1992: 169-178.

855   Sawyer AH, Cardenas MB. Hyporheic flow and residence time distributions in heterogeneous

856   cross-bedded sediment. Water Resources Research 2009; 45.

857   Schade J, Fisher S, Grimm N, Seddon J. The influence of a riparian shrub on nitrogen cycling in

858   a Sonoran Desert stream. Ecology 2001; 82: 3363-3376.

859   Schimel J, Becerra CA, Blankinship J. Estimating decay dynamics for enzyme activities in soils

860   from different ecosystems. Soil Biology and Biochemistry 2017; 114: 5-11.

861   Schoener TW. Resource partitioning in ecological communities. Science 1974; 185: 27-39.

862   Slater LD, Ntarlagiannis D, Day-Lewis FD, Mwakanyamale K, Versteeg RJ, Ward A, et al. Use

863   of electrical imaging and distributed temperature sensing methods to characterize surface

864   water–groundwater exchange regulating uranium transport at the Hanford 300 Area,

865   Washington. Water Resources Research 2010; 46.

866   Sollins P, Homann P, Caldwell BA. Stabilization and destabilization of soil organic matter:

867   mechanisms and controls. Geoderma 1996; 74: 65-105.

868   Stegen JC, Fredrickson JK, Wilkins MJ, Konopka AE, Nelson WC, Arntzen EV, et al.

869   Groundwater–surface water mixing shifts ecological assembly processes and stimulates

870   organic carbon turnover. Nature communications 2016; 7.

871   Stegen JC, Johnson T, Fredrickson JK, Wilkins MJ, Konopka AE, Nelson WC, et al. Influences

872   of organic carbon speciation on hyporheic corridor biogeochemistry and microbial

873   ecology. Nature Communications 2018; 9: 585.

874   Stegen JC, Lin X, Konopka AE, Fredrickson JK. Stochastic and deterministic assembly

875   processes in subsurface microbial communities. The ISME Journal 2012; 6: 1653-1664.

876   Stern N, Ginder-Vogel M, Stegen JC, Arntzen E, Kennedy DW, Larget BR, et al. Colonization

877   habitat controls biomass, composition, and metabolic activity of attached microbial

878   communities in the Columbia River hyporheic corridor. Applied and Environmental

879   Microbiology 2017: AEM. 00260-17.

880   Tfaily MM, Chu RK, Tolić N, Roscioli KM, Anderton CR, Pas□a-Tolić L, et al. Advanced

881   solvent based methods for molecular characterization of soil organic matter by high-

882   resolution mass spectrometry. Analytical chemistry 2015; 87: 5206-5215.

883 Tfaily MM, Chu RK, Toyoda J, Tolić N, Robinson EW, Paša-Tolić L, et al. Sequential extraction

884   protocol for organic matter from soils and sediments using high resolution mass

885   spectrometry. Analytica Chimica Acta 2017; 972: 54-61.

886 Tfaily MM, Podgorski DC, Corbett JE, Chanton JP, Cooper WT. Influence of acidification on

887   the optical properties and molecular composition of dissolved organic matter. Analytica

888   chimica acta 2011; 706: 261-267.

889 Todd-Brown K, Randerson J, Post W, Hoffman F, Tarnocai C, Schuur E, et al. Causes of

890   variation in soil carbon simulations from CMIP5 Earth system models and comparison

891   with observations. Biogeosciences 2013; 10.

892 Tremblay LB, Dittmar T, Marshall AG, Cooper WJ, Cooper WT. Molecular characterization of

893   dissolved organic matter in a North Brazilian mangrove porewater and mangrove-fringed

894   estuaries by ultrahigh resolution Fourier transform-ion cyclotron resonance mass

895   spectrometry and excitation/emission spectroscopy. Marine chemistry 2007; 105: 15-29.

896 Treseder KK. Nitrogen additions and microbial biomass: A meta-analysis of ecosystem studies.

897   Ecology letters 2008; 11: 1111-1120.

898 Tringe SG, Rubin EM. Metagenomics: DNA sequencing of environmental samples. Nature

899   reviews genetics 2005; 6: 805-814.

900 Verheijen LM, Aerts R, Brovkin V, Cavender-Bares J, Cornelissen JH, Kattge J, et al. Inclusion

901   of ecologically based trait variation in plant functional types reduces the projected land

902   carbon sink in an earth system model. Global change biology 2015; 21: 3074-3086.

903 Viant MR. Recent developments in environmental metabolomics. Molecular Biosystems 2008;

904   4: 980-986.

905   Waldrop M, Firestone M. Response of microbial community composition and function to soil

906   climate change. Microbial ecology 2006; 52: 716-724.

907   Wang G, Post WM, Mayes MA. Development of microbial-enzyme-mediated decomposition

908   model parameters through steady-state and dynamic analyses. Ecological Applications

909   2013; 23: 255-272.

910   Wang K, Peng C, Zhu Q, Zhou X, Wang M, Zhang K, et al. Modeling Global Soil Carbon and

911   Soil Microbial Carbon by Integrating Microbial Processes into the Ecosystem Process

912   Model TRIPLEX-GHG. Journal of Advances in Modeling Earth Systems 2017; 9: 2368-

913   2384.

914   Wang Z, Gerstein M, Snyder M. RNA-Seq: a revolutionary tool for transcriptomics. Nature

915   reviews genetics 2009; 10: 57-63.

916   Weintraub MN, Schimel JP. Interactions between carbon and nitrogen mineralization and soil

917   organic matter chemistry in arctic tundra soils. Ecosystems 2003; 6: 0129-0143.

918   Wieder W, Grandy A, Kallenbach C, Bonan G. Integrating microbial physiology and physio-

919   chemical principles in soils with the MIcrobial-MIneral Carbon Stabilization (MIMICS)

920   model. Biogeosciences 2014; 11: 3899-3917.

921   Wieder W, Grandy A, Kallenbach C, Taylor P, Bonan G. Representing life in the Earth system

922   with soil microbial functional traits in the MIMICS model. Geoscientific Model

923   Development 2015a; 8: 1789-1808.

924   Wieder WR, Bonan GB, Allison SD. Global soil carbon projections are improved by modelling

925   microbial processes. Nature Climate Change 2013; 3: 909-912.

926   Wieder WR, Cleveland CC, Smith WK, Todd-Brown K. Future productivity and carbon storage

927   limited by terrestrial nutrient availability. Nature Geoscience 2015b; 8: 441-444.

928   Wieder WR, Hartman MD, Sulman BN, Wang YP, Koven CD, Bonan GB. Carbon cycle

929   confidence and uncertainty: Exploring variation among soil biogeochemical models.

930   Global change biology 2017.

931   Xu X, Schimel JP, Thornton PE, Song X, Yuan F, Goswami S. Substrate and environmental

932   controls on microbial assimilation of soil organic carbon: a framework for Earth system

933   models. Ecology letters 2014; 17: 547-555.

934   Yin Y, Mao X, Yang J, Chen X, Mao F, Xu Y. dbCAN: a web resource for automated

935   carbohydrate-active enzyme annotation. Nucleic acids research 2012; 40: W445-W451.

936   Zachara JM, Long PE, Bargar J, Davis JA, Fox P, Fredrickson JK, et al. Persistence of uranium

937   groundwater plumes: Contrasting mechanisms at two DOE sites in the groundwater–river

938   interaction zone. Journal of contaminant hydrology 2013; 147: 45-72.

939   Zarnetske JP, Haggerty R, Wondzell SM, Baker MA. Dynamics of nitrate production and

940   removal as a function of residence time in the hyporheic zone. Journal of Geophysical

941   Research: Biogeosciences 2011; 116.

942   Zhang D, Hui D, Luo Y, Zhou G. Rates of litter decomposition in terrestrial ecosystems: global

943   patterns and controlling factors. Journal of Plant Ecology 2008; 1: 85-93.

944